Cancer Letters 383 (2016) 243–249

Contents lists available at ScienceDirect

Cancer Letters

journal homepage: www.elsevier.com/locate/canlet

Original Article

Dye-conjugated single-walled carbon nanotubes induce photothermal therapy under the guidance of near-infrared imaging

Xiaoyuan Liang [a, b, c, 1], Wenting Shang [b, c, 1], Chongwei Chi [b, c], Chaoting Zeng [a], Kun Wang [b, c], Chihua Fang [a], Qingshan Chen [a], Huiyu Liu [d], Yingfang Fan [a, *], Jie Tian [b, c, *]

[a] Department of Hepatobiliary Surgery, Zhujiang Hospital, Southern Medical University, Guangzhou 510280, China
[b] Key Laboratory of Molecular Imaging, Institute of Automation, Chinese Academy of Sciences, Beijing 100190, China
[c] Beijing Key Laboratory of Molecular Imaging, Beijing 100190, China
[d] College of Life Science and Technology, Beijing University of Chemical Technology, Beijing, China

ARTICLE INFO

Article history:
Received 5 August 2016
Received in revised form
1 September 2016
Accepted 2 September 2016

Keywords:
Photothermal therapy (PTT)
Near-infrared imaging (NIR)
Single-walled carbon nanotubes
Cy5.5

ABSTRACT

Recently, photothermal therapy (PTT) has become viewed as an ideal auxiliary therapeutic treatment for cancers. However, the development of safe, convenient, and highly effective photothermal agents remains a great challenge. In this study, we prepared single-walled carbon nanotubes (SWNTs) for PTT against breast tumors under the guidance of infrared fluorescent cyanines. Tumors were accurately located using near-infrared imaging (NIR) and then exposed to laser irradiation. Both the *in vivo* and *in vitro* results showed that the SWNTs have high stability and low cytotoxicity. Introducing polyethylene glycol into our nanoparticles increased the blood-circulation time. Our *in vivo* results further showed that Cy5.5-conjugated SWNTs mediated PTT, resulting in efficient tumor suppression in mice under the guidance of near-infrared imaging. Due to the small amount of absorption at 808-nm, Cy5.5 increased the efficiency of PTT. Breast tumors significantly shrunk after irradiation under the 808-nm near-infrared laser. The treated mice developed scabs, but otherwise recovered after 15 days, and their physical conditions restored gradually. These data indicate that our unique photothermal-responsive SWNT-Cy5.5-based theranostic agent can serve as a promising candidate for PTT.

Introduction

As a new trend in treatment, precision medicine has drawn much attention [1,2]. The integration of diagnosis and treatment, which can improve the survival rate and quality of life of post-operative patients, has provided an attractive avenue for detecting and treating cancer [3,4]. Imaging-guided photothermal therapy (PTT), a novel adjuvant therapeutic method of precision therapy, could be used to completely eliminate remaining cancer cells under precise guidance in the future [5–7]. PTT accurately transfers the absorbed light into thermal energy and generates local hyperthermia in the tumor mass to ablate cancer cells without causing damage to the surrounding normal tissues [8–10]. However, PTT shows poor accuracy in killing cancer cells without the use of contrast agents. Therefore, a precise tumor ablation combined with an accurate imaging guide is of significance in PTT [11].

Recently, contrast agents utilized in PTT, which can transfer light energy into thermal energy, have been effectively employed for accurate disease diagnosis and therapy [12–14]. Nanoparticles, especially theranostic nanoparticles, which have combined therapeutic and diagnostic capabilities, have promise in providing new therapeutic strategies in the biomedical field [15–17]. Cai et al. used a novel method to load indocyanine green into hybrid polypeptide micelles for tumor imaging and PTT [18]. Li et al. used hyaluronic acid to modify core/shell Fe_3O_4@Au for tumor multimodal imaging and PTT [19]. However, the disadvantages of contrast agents have limited their applications. NIR dyes have a wide optical-absorption range, which causes energy losses and the inability to achieve a powerful heating effect [20,21]. Metal NPs can efficiently transform light into thermal energy, but they generally possess potential long-term toxicity *in vivo* [22]. Therefore, ideal contrast agents are urgently needed for accurate PTT.

* Corresponding authors..
E-mail addresses: fanyf068700@sina.com (Y. Fan), jie.tian@ia.ac.cn (J. Tian).
[1] The parallel first authors.

http://dx.doi.org/10.1016/j.canlet.2016.09.006
0304-3835/

They should have a strong characteristic absorption peak in the NIR region, low toxicity, and improved biocompatibility over the current contrast agents. Because of the unique physical and chemical properties of carbon nanotubes in general and single-walled carbon nanotubes (SWNTs) in particular, SWNTs have generated substantial interest in nanomedicine for applications in thermal therapy, biosensors, tissue engineering, and cancer imaging [23–26]. The surfaces of SWNTs can be easily modified, such as with polyethylene glycol (PEG), polyvinyl pyrrolidone (PVP); SWNTs can exhibits high solubility and stability in physiological solutions [27,28]. When conjugated with a fluorescence dye, SWNTs can be used to detect tumors. Therefore, SWNTs have excellent biocompatibility and paintability [29]. In addition, SWNTs can be readily taken up by cells and are non-cytotoxic within a certain concentration range if suitably functionalized [30]. SWNTs can absorb NIR laser light to generate a local high temperature, which may kill the cancer cells [31,36]. Thus, SWNTs can be used as accurate agents for PTT.

In this study, we prepared the contrast agent SWNT-cyanine 5.5 (Cy5.5) for accurate diagnosis and treatment by taking advantage of optical imaging and photothermal therapy in the NIR region. Due to its adequate penetration depth, Cy5.5 was employed to locate the tumor site, monitor the biodistribution of SWNTs, and find an optimal time-window for PTT [32,33]. SWNTs have a strong ability to transform incident 808-nm NIR light into heat energy and ablate cancer cells [34]. Furthermore, Cy5.5 emits NIR light of 710 nm for tumor imaging. Due to its accurate imaging properties and effective photothermal therapy, such as low toxicity and enhanced biocompatibility, SWNT-Cy5.5 is an appealing candidate for future translation of nanomedicine.

Materials and methods

Materials

SWNTs 1–3 μm in length and 1–2 nm in diameter were purchased from Chengdu Organic Chemicals Co., Ltd (95% pure). Distearoyl phosphoethanolamine-PEG WM3500 (DSPE-PEG WM3500) was obtained from Beijing Chemgen Pharma Co. Ltd. Cy5.5-NHS was provided by Tianjin Biolite Biotech Co., Ltd. Dulbecco's Modified Eagle's Medium (DMEM) cell culture medium, penicillin, streptomycin and fetal bovine serum (FBS), PBS, and trypsin + EDTA were obtained from Gibco Invitrogen. BALB/c mice (4–6 weeks, n = 20) were provided by Beijing Vital River Laboratory Animal Technology Co., Ltd. All experimental protocols were approved by the Institutional Animal Care and Ethics Committee of Zhujiang Hospital of Southern Medical University, and all methods were performed in accordance with the approved guidelines.

MCF-7 is a human breast adenocarcinoma cancer cell line purchased from American Type Culture Collection (ATCC). Regular MCF-7 cells were cultured in DMEM, supplemented with 10% FBS, penicillin, and streptomycin. All cells were cultured in an atmosphere of 5% CO_2 at 37 °C. All experiments were performed on cells in the logarithmic phase of growth.

Methods

Probe synthesis

SWNT-PEG was synthesized as described previously [36]. SWNTs (0.5 g) were added into a 3-necked flask (100 mL) containing 40 mL of 3: 1 (v: v) nitric acid and concentrated sulfuric acid at room temperature. The suspension was sonicated for 30 min before being heated to 110 °C and refluxed under vigorous magnetic stirring for 110 h until the SWNTs dissolved completely. SWNTs were centrifuged and washed with water and ethanol, and dried at 80 °C for 24 h. A water-soluble carboxylic SWNT powder was obtained.

Modified SWNTs (0.5 g) were added to 1 mL deionized water. DSPE-PEG WM3500 (500 mg) was added and mixed by vibrating for 30 min. Then, 20 μg of Cy5.5 was added. The product was isolated by centrifugation at 8500 rpm for 15 min and dispersed into deionized water. The obtained material was denoted as SWNT-Cy5.5. A schematic representation of the preparation procedure is shown in Fig. S1.

Cytotoxicity assay

MCF-7 cell viabilities were determined in MTT assays. MCF-7 cells were seeded into a 96-well tissue culture plate at a density of 1×10^4 cells per well in 200 μL of cell culture medium, which method is described previously [38]. The cells reached 60–80% confluency after incubation 24 h. Then, the cells were incubated with different doses of free SWNTs, SWNT-PEG, or SWNT-Cy5.5. After 24 h incubation, cytotoxicity was evaluated in MTT assays and expressed as the relative cell viability after normalization with untreated cell controls.

Temperature variation of SWNT-Cy5.5 after laser irradiation

To quantitatively determine the thermal properties of SWNTs after laser irradiation, the nanotubes were dispersed in PBS and irradiated with a laser (1 W cm^{-2} or 2 W cm^{-2}) for 4 min. Temperature changes were monitored with an infrared video camera every min.

To explore the effect of Cy5.5, probes with the same Cy5.5 concentration were irradiated with similar laser powers for 5 min. Temperature changes were monitored with infrared video camera every min.

Cellular uptake of SWNT-Cy5.5

Probe internalization by MCF-7 cells was detected as follows. MCF-7 cells were incubated in DMEM with 10% FBS, 1% penicillin, and 1% streptomycin. Cells were seeded in 6-well tissue culture plates at a density of 1×10^6 cells per well in 5 mL of cell culture medium. Various nanoprobes were added when the cells reached 60–80% confluency after approximately 24 h. The cells were then incubated with different concentrations of SWNT-Cy5.5. After 24 h, the results were observed with a home-made fluorescence microscope.

PTT effect on cells in vitro

To quantitatively explore the PTT function of SWNT-Cy5.5 on the viability of breast cancer cells, MCF-7 cells were pre-incubated with different concentrations of SWNT, SWNT-PEG, or SWNT-Cy5.5 in 96-well plates. After 24 h, the MCF-7 cells were treated with an 808-nm laser at a laser power output of 1 W cm^{-2} or 2 W cm^{-2} for 4 min. When the high temperature of the plates caused by irradiation decreased after 4 h, the viability of the laser-irradiated cells was evaluated by performing an MTT assay.

Preparation of tumor-bearing mice

Subcutaneously implanted tumor model in nude mice with human breast cell carcinoma were used in the experiments.

Human breast cell carcinoma, MCF-7 cancer cell line, was cultured in DMEM, supplemented with 10% FBS, 1% penicillin and streptomycin under 5% CO2 at 37 °C. The MCF-7 cells (1 × 106 cells) were suspended in 150 μL PBS and subcutaneously injected into the right armpit of female BALB/c mice of each group (4–6 weeks, n = 20). The life quality of mice was observed continuously till tumors were prepared for experiments. When the tumors grew to approximately 4 mm in diameter and the volumes grew to about 150–200 mm^3, the mice were divided into four groups to be used *in vivo* study. The tumor volume, monitored with a digital caliper, was calculated by formula V = a × b × b/2 (a, longest dimension; b, shortest dimension).

Biodistribution of SWNT-Cy5.5 and accurate diagnosis in vivo

To confirm the best time for PTT, SWNT-Cy5.5 was injected into tumor-bearing mice through the tail vein at a concentration of 0.8 mg kg^{-1}. The probe biodistribution was observed using a Living Imaging System (IVIS, Caliper Sciences IVIS Spectrum 3D) for 48 h.

PTT of SWNT-Cy5.5 under NIR laser irradiation in vivo

The photothermal effects of SWNTs were measured by an IR thermal imaging system during the irradiation of each mouse. At first, 12 tumor-bearing mice were randomly divided into 4 groups (SWNT-Cy5.5 treated, SWNT-Cy5.5-untreated, PBS-treated, and PBS-untreated) according to their original weights and tumor volumes, which were recorded at the same time. Then, SWNT-Cy5.5 was dispersed in 200 μL PBS and injected at a concentration of 0.8 mg kg^{-1} into mice in the SWNTs groups. In parallel, 200 μL PBS (without SWNTs) was injected into the PBS groups. The results of the biodistribution experiments showed that approximately 8 h post-injection was the best time for irradiation. Finally, the tumors of 6 mice were exposed to 808-nm laser irradiation (2 W cm^{-2} for 5 min) at a distance of 3 cm to avoid damaging normal tissues. The increase in temperature of the tumor skin before and during irradiation was recorded by an infrared video camera every min. The quality of life of the treated mice was continuously observed after therapy.

Results and discussion

Characterization of SWNT-Cy5.5

SWNTs and modified SWNTs were characterized by transmission electron microscopy (TEM), described in the supporting information. TEM images (Fig. 1A and B) showed that the morphologies of SWNTs did not change substantially after modification. As Fig. 1B shows, the SWNTs showed high dispersibility following carboxylation. Thermo Gravimetric Analyzer (TGA) analysis of SWNT-Cy5.5 (Fig. S2) indicated a 2-fold reduction in weight based

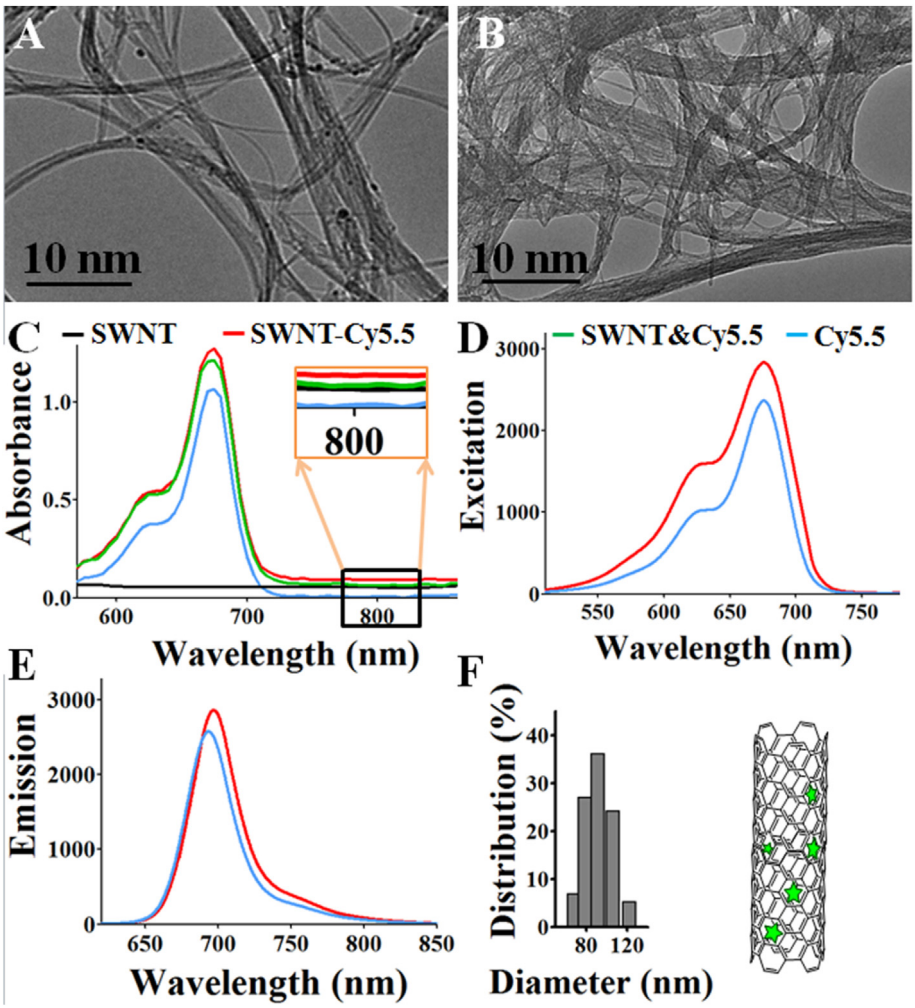

Fig. 1. Characterization of SWNT-Cy5.5. (A) and (B) TEM images of SWNTs and functionalized SWNTs. (C) Visible absorption spectra of SWNT, Cy5.5, SWNT&Cy5.5 and SWNT-Cy5.5. Excitation (D) and emission (E) spectra of SWNT-Cy5.5 and Cy5.5. (F) Hydrodynamic size distribution of the nanoparticles. The green stars represent conjugated Cy5.5 molecules in the SWNTs. (For interpretation of the references to colour in this figure legend, the reader is referred to the web version of this article.)

on 38.4% loading efficacy. Fig. 1C demonstrates the absorbance of SWNT, Cy5.5, SWNT&Cy5.5 and SWNT-Cy5.5, respectively. Compare with SWNT (black bar), cy5.5 (blue bar), SWNT&Cy5.5 (green bar) absorbance is only simple superposition. However, SWNT conjugated with Cy5.5 (SWNT-Cy5.5) improve whole optical absorbance, especially wavelength > 700 nm region. Fig. 1D and E demonstrate that the respective excitation (675 nm) and emission (701 nm) spectra of Cy5.5 were nearly unaffected by the conjugation to SWNTs. The excitation spectrum (Fig. 1D) showed an obvious redshift of approximately 7 nm. This was probably attributable to Cy5.5 conjugation and indicated that deeper tissues could be seen than with previous contrast agents, as the redshift of SWNT-Cy5.5 increased the penetrating depth. Fig. 1F shows that the hydrodynamic sizes of SWNT-Cy5.5 particles were in the range of 54–118 nm, which can passively target tumor issues through the enhanced permeation and retention (EPR) effect [35]. The amount of Cy5.5 conjugated to the SWNTs was estimated using formula (1) and (2) in the supporting information file.

In vitro NIR effect of SWNTs and SWNT-Cy5.5

The NIR effect of the probes was studied to identify the proper laser power, irradiation time, and concentration *in vivo* (Fig. 2). Phosphate-buffered saline (PBS) was used as the negative control. Previous studies provided evidence that cancer cells can be ablated when the temperature exceeds 42.5 °C [37]. SWNT-Cy5.5 was prepared at 5 different concentrations, which showed benign dispersibility and could be uniformly heated when irradiated by a laser (Fig. 2C). Fig. 2A shows that, with increasing laser power, the temperature can reach approximately 55 °C, even up to 90 °C under 2 W cm^{-2} in Fig. 2B. The finding indicates that SWNTs dispersed in aqueous solution at different concentrations are capable of killing cancer cells, even at very low concentrations. With increasing SWNT-Cy5.5 concentrations, the temperature of the solution increased noticeably. Fig. 2A and B shows that, compared with the experimental group, the temperature of the PBS group showed no obvious changes with different laser powers. As same density of 0.4 mg mL^{-1}, Cy5.5 showed a small temperature increase, approximately 10 °C (Fig. 2D), which was probably due to the integral raise of absorption ability after conjugated to Cy5.5 showed in Fig. 1C. However, Cy5.5 did not show robust heating effects under irradiation at 808-nm. When conjugated to SWNTs, enhanced heating effects were clearly displayed (Fig. 2D, ΔT).

The time of laser exposure and the probe concentration were found to be important factors for PTT. Over time, the laser power

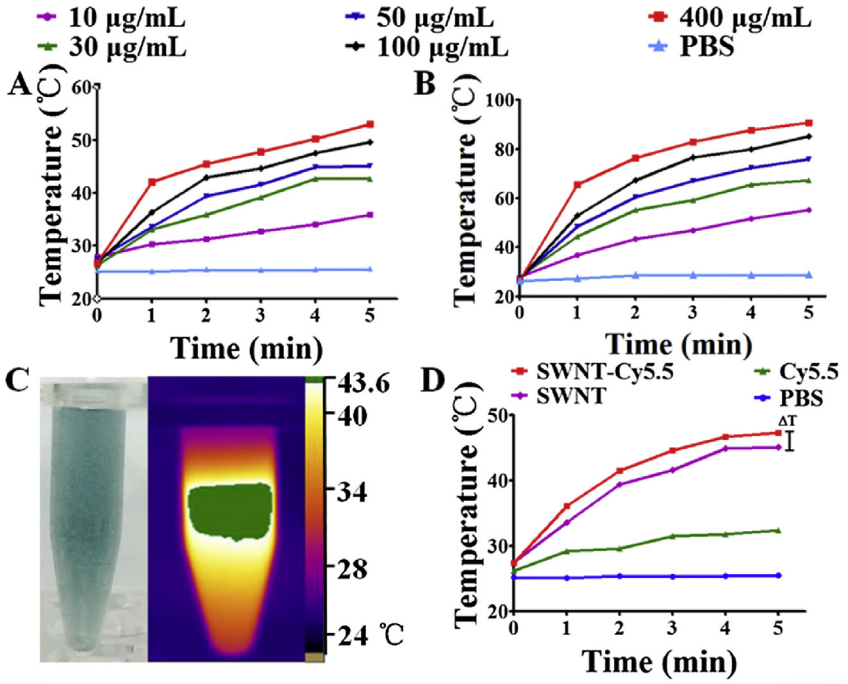

Fig. 2. Photothermal effects of probes *in vitro*. The effects of varying the SWNT-Cy5.5 concentration and laser-irradiation power from 1 W cm^{-2} (A) to 2 W cm^{-2} (B) are shown. (C) SWNT-Cy5.5 before and after a 1-min irradiation at 808-nm. (D) Temperature variations for different probes following laser irradiation (ΔT) means the raise of absorption ability.

and concentration both increased and SWNT-Cy5.5 showed strong optical absorbance, which suggested that the potential of these nanoparticles in PTT and the enhancing effects of SWNT-Cy5.5 should be explored further in cells.

In vitro MCF-7 uptake, cytotoxicity, and ablation

The *in vitro* cellular uptake of SWNT-Cy5.5 could be seen clearly using a home-made fluorescence microscope. SWNT-Cy5.5 was internalized by MCF-7 cells (Fig. 3A). SWNT-Cy5.5 inside the MCF-7 cells could be excited by a 701 nm light source. In contrast, minimal background fluorescence was observed, suggesting that SWNT-Cy5.5 can be used for NIR cellular imaging or for observing tumors in a living body.

The toxicity was tested using a microplate reader to ensure the safety of the probe for applications with live recipients and to provide a moderate dosage that could be used *in vivo*. Fig. 3B shows that SWNT-Cy5.5 did not show higher toxicity than SWNTs or Cy5.5

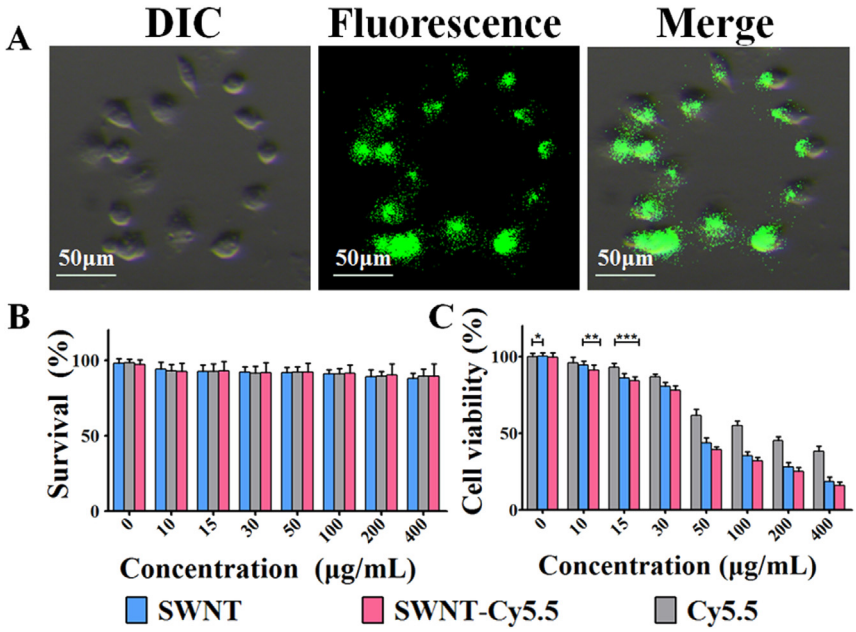

Fig. 3. Images of MCF-7 cells, cell toxicity, and ablation *in vitro* following incubation with SWNT-Cy5.5. (A) DIC, fluorescent, and merged images after incubation with SWNT-Cy5.5. Scale bar, 50 μm. (B) Toxicity test results of SWNT, SWNT-Cy5.5, and Cy5.5 ($P > 0.05$). (C) Cell viability of MCF-7 cells incubated with SWNT, Cy5.5, and SWNT-Cy5.5 after PTT ($P^* < 0.01$, $P^{**} < 0.001$, $P^{***} < 0.001$).

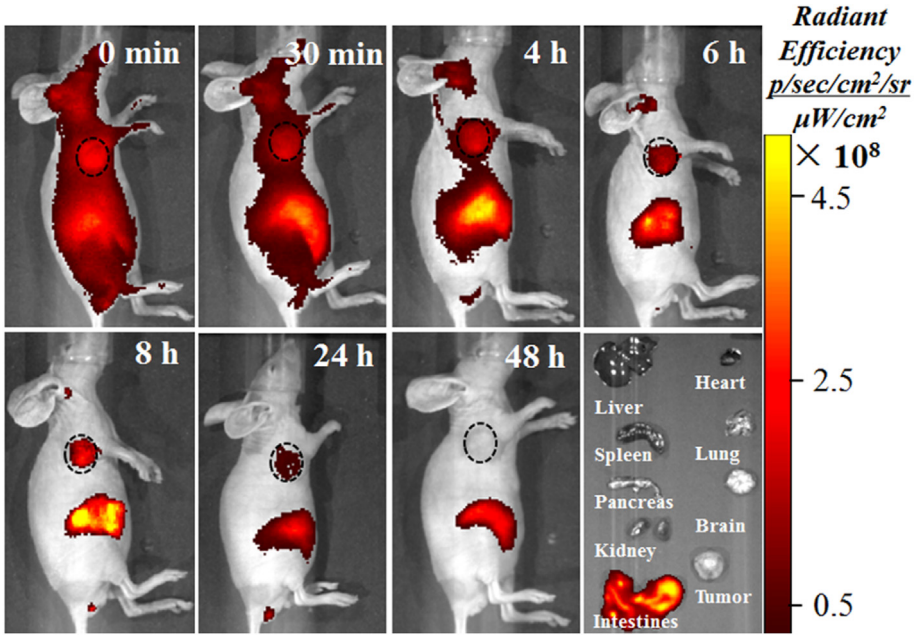

Fig. 4. The distribution and biodistribution of SWNT-Cy5.5 after tail vein injection. The final picture shows the approximate SWNT-Cy5.5 concentration in different organs at 48 h post-injection.

alone, which are produced during the preparation of contrast agents even at a concentration of 400 μg mL^{-1} ($P > 0.05$). Toxicity testing *in vivo* was also conducted. As Fig. S3 shows, toxicity *in vivo* before and after probe injection showed marginal differences, indicating that SWNT-Cy5.5 had almost no toxicity to cells and living mice.

When irradiated with an 808-nm laser light, contrast agents incubated with MCF-7 cells showed a clear disruption to cells in SWNT group and displayed strong optical absorbance in the NIR range (Fig. 3C). However, MCF-7 cells exposed to SWNTs or Cy5.5 ($P^* < 0.01$, $P^{**} < 0.001$) did not show lower viability than cells exposed to SWNT-Cy5.5 ($P^{***} < 0.001$), which also indicated the enhancing effects of SWNTs and Cy5.5. Overall, our data indicated that SWNT-Cy5.5 showed potential for transforming light into thermal energy.

In vivo NIR imaging and biodistribution of SWNT-Cy5.5

NIR imaging of SWNT-Cy5.5 in the living mice enables accurate tumor localization and a proper healing time for PTT [39]. Mice for this experiment were planted subcutaneous breast cancer tumor. Fig. 4 shows that the circulation time of SWNT-Cy5.5 in the blood was up to 48 h. SWNT-Cy5.5 was concentrated mostly at the tumors at 6–8 h post-tail vein injection according to EPR effect, as determined by continual monitoring of changes in fluorescence intensity. After a 48-h biodistribution, the mouse was necropsied

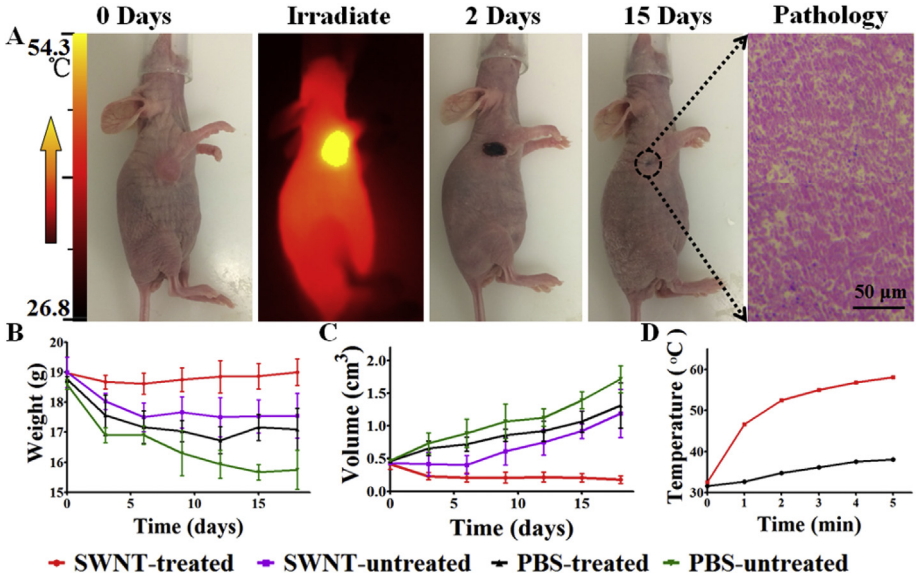

Fig. 5. Photothermal effects of SWNT-Cy5.5 in mice exposed to NIR laser irradiation. (A) Nude mouse with a transplanted subcutaneous sarcoma before, during, and after laser irradiation. The picture on the left shows the pathology of the irradiated tumor site. Variation in mouse weights (B) and tumor volumes (C) after irradiation. (D) Temperature variations in the SWNT-Cy5.5 and PBS groups.

and the organs and tumors were used to study metabolic pathways by measuring the fluorescence intensity. SWNT-Cy5.5 was excreted through the intestines and the metabolic pathways indicated a low toxicity to the liver and normal tissues, which ensured the safety of SWNT-Cy5.5 to the living body. We choose three regions of interest (ROIs; 0.2 mm^2), including intestines, liver and tumor ROI in each timing (Fig. 4). ROIs were evaluated to show the accumulation of SWNT-Cy5.5 (Fig. S5) which verifies previous assumption. Furthermore, this experiment indicated that 6–8 h post-injection was the best time for exposing tumors to laser light.

PTT of tumors in vivo

Using an appropriate time, contrast agent concentration, and irradiation power, the mouse groups were treated with SWNT-Cy5.5 + PTT (SWNT-treated), SWNT-Cy5.5 alone (SWNT-untreated), PBS + PTT (PBS-treated), and PBS alone (PBS-untreated). Mice treated with or without SWNT-Cy5.5 were exposed to 808-nm laser light. Variations in temperature during irradiation were monitored using an IR thermal-imaging system. The temperature of the tumor in the SWNT-treated group increased to 43 °C after laser irradiation at 2 W cm^{-2} for 1 min. The temperature further increased to 58 °C after irradiation for 4 min (Fig. 5D). No significant change in the temperature of the control group was observed and the temperature was stable at approximately 38–39 °C. Fig. 5A shows that the temperature of the tumor increased noticeably. The cancer cells were killed due to the high temperature. Two days after the irradiation, the site exposed to the laser light was covered by a crust with no blisters or fluid. At 15 days post-treatment, the scab fell off and fresh, completely healed skin was seen underneath.

The mice weights and tumor volumes were recorded directly after irradiation every 3 days. As shown in Fig. 5B and C, the weights of mice in the SWNT-Cy5.5-treated group increased gradually, and the tumor volume decreased gradually (Fig. S4A). Mouse survival was monitored to evaluate the quality of life after treatment (Fig. S4B). However, no obvious anti-tumor effect was observed for the PBS-treated group, indicating that PBS + laser exposure could not ablate cancer cells effectively. The tumor volumes in the untreated group continued to grow, resulting in the death of the mice.

Conclusions

In conclusion, tumors can be treated by PTT after detected by NIR fluorescence imaging using SWNT-Cy5.5. This approach provides an interesting method for locating tumors and facilitating therapy after selecting the corresponding treatment. Due to its appropriate size, SWNT-Cy5.5 can be easily internalized by cells and then utilized for light-thermal energy conversion when the cells are irradiated. In addition, SWNT-Cy5.5 can accumulate in tumors to avoid damaging normal tissues during irradiation. Interestingly, conjugated with Cy5.5, SWNT-Cy5.5 was found an enhancing effect during PTT irradiation. In summary, SWNT-Cy5.5 has the potential to facilitate numerous applications in clinical auxiliary treatment.

To develop the best support therapy, further study of florescence imaging and photothermal therapy applied to the living body are urgently needed. Thus, SWNT can serve as materials for theranostic nanomedicine applications in clinical settings.

Author contributions

Xiaoyuan Liang and Wenting Shang conceived and designed the experiments; Xiaoyuan Liang, Wenting Shang, and Chaoting Zeng performed the experiments; Xiaoyuan Liang, Qingshan Chen, and Chihua Fang analyzed the data; Chongwei Chi, Kun Wang, and Huiyu Liu contributed materials and analysis tools; and Xiaoyuan Liang, Yingfang Fan, and Jie Tian wrote the paper.

Acknowledgments

This paper was supported by: 1. The National High Technology Research and Development Program of China (863 Program; Grant No. 2012AA021105). 2. The National Natural Science Foundation of China under Grant Nos. 81501540 and 61501462. 3. Natural Science Foundation of China-Guangdong United Funds (Grant No. U1401254). 4. The Science and Technology Planning Project of Guangdong Province, China (Grant No. 2015B031800091). 5. The Guangdong Province Science and Technology Plan Project (Grant No. 2016A020220013). 6. The Strategic Priority Research Program from Chinese Academy of Sciences (XDB02060010).

Conflicts of interest

The authors declare no conflict of interest.

Appendix A. Supplementary data

Supplementary data related to this article can be found at http://dx.doi.org/10.1016/j.canlet.2016.09.006.

References

[1] S. Derks, A.H.G. Cleven, V. Melotte, K.M. Smits, J.C. Brandes, N. Azad, W. van Criekinge, A.P. de Bruine, J.G. Herman, M. van Engeland, Emerging evidence for CHFR as a cancer biomarker: from tumor biology to precision medicine, Cancer Metast Rev. 33 (2014) 161–171.
[2] D. Peer, Precision medicine – delivering the goods? Cancer Lett. 352 (2014) 2–3.
[3] J.P. Wang, R. Yan, F. Guo, M. Yu, F.P. Tan, N. Li, Targeted lipid-polyaniline hybrid nanoparticles for photoacoustic imaging guided photothermal therapy of cancer, Nanotechnology 27 (2016).
[4] A.C.P. Nazario, G. Facina, J.R. Filassi, Breast cancer: news in diagnosis and treatment, Rev. Assoc. Med. Bras. 61 (2015) 543–552.
[5] J. Song, J. Qu, M.T. Swihart, P.N. Prasad, Near-IR responsive nanostructures for nanobiophotonics: emerging impacts on nanomedicine, Nanomedicine 12 (2016) 771–788.
[6] R.K. Kannadorai, G.G.Y. Chiew, K.Q. Luo, Q. Liu, Dual functions of gold nanorods as photothermal agent and autofluorescence enhancer to track cell death during plasmonic photothermal therapy, Cancer Lett. 357 (2015) 152–159.
[7] G. Yuan, Y.J. Yuan, K. Xu, Q. Luo, Biocompatible PEGylated Fe3O4 nanoparticles as photothermal agents for near-infrared light modulated cancer therapy, Int. J. Mol. Sci. 15 (2014) 18776–18788.
[8] B. Liu, C.X. Li, Z.Y. Cheng, Z.Y. Hou, S.S. Huang, J. Lin, Functional nanomaterials for near-infrared-triggered cancer therapy, Biomateri. Sci. 4 (2016) 890–909.
[9] L. Cheng, C. Wang, L.Z. Feng, K. Yang, Z. Liu, Functional nanomaterials for phototherapies of Cancer, Chem. Rev. 114 (2014) 10869–10939.
[10] J. Lee, D.K. Chatterjee, M.H. Lee, S. Krishnan, Gold nanoparticles in breast cancer treatment: promise and potential pitfalls, Cancer Lett. 347 (2014) 46–53.
[11] D.E. Lee, H. Koo, I.C. Sun, J.H. Ryu, K. Kim, I.C. Kwon, Multifunctional nanoparticles for multimodal imaging and theragnosis, Chem. Soc. Rev. 41 (2012) 2656–2672.
[12] A. Espinosa, R. Di Corato, J. Kolosnjaj-Tabi, P. Flaud, T. Pellegrino, C. Wilhelm, Duality of iron oxide nanoparticles in cancer therapy: amplification of heating efficiency by magnetic hyperthermia and photothermal bimodal treatment, ACS Nano 10 (2016) 2436–2446.
[13] C.P. Epperla, O.Y. Chen, H.C. Chang, Gold/diamond nanohybrids may reveal how hyperlocalized hyperthermia kills cancer cells, Nanomedicine 11 (2016) 443–445.
[14] X.S. Ye, H. Shi, X.X. He, Y.R. Yu, D.G. He, J.L. Tang, Y.L. Lei, K.M. Wang, Cu-Au alloy nanostructures coated with aptamers: a simple, stable and highly effective platform for in vivo cancer theranostics, Nanoscale 8 (2016) 2260–2267.
[15] S.S. Kelkar, T.M. Reineke, Theranostics: combining imaging and therapy, Bioconjug Chem. 22 (2011) 1879–1903.
[16] S. Marchesan, M. Prato, Nanomaterials for (nano)medicine, ACS Med. Chem. Lett. 4 (2013) 147–149.
[17] A. Wicki, D. Witzigmann, V. Balasubramanian, J. Huwyler, Nanomedicine in cancer therapy: challenges, opportunities, and clinical applications, J. Control Release 200 (2015) 138–157.

[18] L. Wu, S.T. Fang, S. Shi, J.Z. Deng, B. Liu, L.T. Cai, Hybrid polypeptide micelles loading indocyanine green for tumor imaging and photothermal effect study, Biomacromolecules 14 (2013) 3027–3033.
[19] J.C. Li, Y. Hu, J. Yang, P. Wei, W.J. Sun, M.W. Shen, G.X. Zhang, X.Y. Shi, Hyaluronic acid-modified Fe3O4@Au core/shell nanostars for multimodal imaging and photothermal therapy of tumors, Biomaterials 38 (2015) 10–21.
[20] M.B. Zheng, P.F. Zhao, Z.Y. Luo, P. Gong, C.F. Zheng, P.F. Zhang, C.X. Yue, D.Y. Gao, Y.F. Ma, L.T. Cai, Robust ICG theranostic nanoparticles for folate targeted cancer imaging and highly effective photothermal therapy, ACS Appl. Mater Interfaces 6 (2014) 6709–6716.
[21] Z.H. Sheng, D.H. Hu, M.M. Xue, M. He, P. Gong, L.T. Cai, Indocyanine green nanoparticles for theranostic applications, Nano-Micro Lett. 5 (2013) 145–150.
[22] S.D. Brown, P. Nativo, J.A. Smith, D. Stirling, P.R. Edwards, B. Venugopal, D.J. Flint, J.A. Plumb, D. Graham, N.J. Wheate, Gold nanoparticles for the improved anticancer drug delivery of the active component of oxaliplatin, J. Am. Chem. Soc. 132 (2010) 4678–4684.
[23] A.C. Tripathi, S.A. Saraf, S.K. Saraf, Carbon nanotropes: a contemporary paradigm in drug delivery, Materials 8 (2015) 3068–3100.
[24] S.F. Oliveira, G. Bisker, N.A. Bakh, S.L. Gibbs, M.P. Landry, M.S. Strano, Protein functionalized carbon nanomaterials for biomedical applications, Carbon 95 (2015) 767–779.
[25] Y.M. Yu, T. Zhang, L.B. Gan, Synthesis of open-cage fullerenes with 4-alkynylphenyl groups on the rim of the orifice, Fuller Nanotub Car N. 22 (2014) 54–60.
[26] Z.M. Ou, B.Y. Wu, D. Xing, F.F. Zhou, H.Y. Wang, Y.H. Tang, Functional single-walled carbon nanotubes based on an integrin alpha(v)beta(3) monoclonal antibody for highly efficient cancer cell targeting, Nanotechnology 20 (2009).
[27] G. Bisker, J. Dong, H.D. Park, N.M. Iverson, J. Ahn, J.T. Nelson, M.P. Landry, S. Kruss, M.S. Strano, Protein-targeted corona phase molecular recognition, Nat. Commun. 7 (2016).
[28] D.P. Salem, M.P. Landry, G. Bisker, J. Ahn, S. Kruss, M.S. Strano, Chirality dependent corona phase molecular recognition of DNA-wrapped carbon nanotubes, Carbon 97 (2016) 147–153.
[29] C. Bussy, K.T. Al-Jamal, J. Boczkowski, S. Lanone, M. Prato, A. Bianco, K. Kostarelos, Microglia determine brain region-specific neurotoxic responses to chemically functionalized carbon nano tubes, ACS Nano 9 (2015) 7815–7830.
[30] K. Kostarelos, L. Lacerda, G. Pastorin, W. Wu, S. Wieckowski, J. Luangsivilay, S. Godefroy, D. Pantarotto, J.P. Briand, S. Muller, M. Prato, A. Bianco, Cellular uptake of functionalized carbon nanotubes is independent of functional group and cell type, Nat. Nanotechnol. 2 (2007) 108–113.
[31] C. Liang, S. Diao, C. Wang, H. Gong, T. Liu, G.S. Hong, X.Z. Shi, H.J. Dai, Z. Liu, Tumor metastasis inhibition by imaging-guided photothermal therapy with single-walled carbon nanotubes, Adv. Mater 26 (2014) 5646–5652.
[32] A. Abulrob, E. Brunette, J. Slinn, E. Baumann, D. Stanimirovic, In vivo optical imaging of ischemic blood-brain barrier disruption, Methods Mol. Biol. 763 (2011) 423–439.
[33] H. Gong, R. Peng, Z. Liu, Carbon nanotubes for biomedical imaging: the recent advances, Adv. Drug Deliv. Rev. 65 (2013) 1951–1963.
[34] G. Feng, H.Y. Zhang, D.V. Papavassiliou, K. Bui, C. Lim, H.M. Duong, Mesoscopic modeling of cancer photothermal therapy using single-walled carbon nanotubes and near infrared radiation: insights through an off-lattice Monte Carlo approach, Nanotechnology 25 (2014).
[35] H. Maeda, J. Wu, T. Sawa, Y. Matsumura, K. Hori, Tumor vascular permeability and the EPR effect in macromolecular therapeutics: a review, J. Control Release 65 (2000) 271–284.
[36] K. Welsher, Z. Liu, D. Daranciang, H. Dai, Selective probing and imaging of cells with single walled carbon nanotubes as near-infrared fluorescent molecules, Nano Lett. 8 (2008) 586–590.
[37] A. Mazumder, G.V. Shivashankar, Gold-nanoparticle-assisted laser perturbation of chromatin assembly reveals unusual aspects of nuclear architecture within living cells, Biophys. J. 93 (2007) 2209–2216.
[38] C.T. Zeng, W.T. Shang, K. Wang, C.W. Chi, X.H. Jia, C. Fang, D. Yang, J.Z. Ye, C.H. Fang, J. Tian, Intraoperative identification of liver Cancer microfoci using a targeted near-infrared fluorescent probe for imaging-guided surgery, Sci. Rep. 6 (2016), http://dx.doi.org/10.1038/srep21959.
[39] K. Wang, C.W. Chi, Z.H. Hu, M.H. Liu, H. Hui, W.T. Shang, D. Peng, S. Zhang, J.Z. Ye, H.X. Liu, J. Tian, Optical molecular imaging frontiers in oncology: the pursuit of accuracy and sensitivity, Engineering 1 (2015) 309–323.